A&A 468, 649–655 (2007)
DOI: 10.1051/0004-6361:20077298

Astronomy & Astrophysics

Mass fluxes for O stars

L. B. Lucy

Astrophysics Group, Blackett Laboratory, Imperial College London, Prince Consort Road, London SW7 2AZ, UK
e-mail: l.lucy@imperial.ac.uk

Received 14 February 2007 / Accepted 26 March 2007

ABSTRACT

The theory of moving reversing layers for hot stars is updated to include an extensive line list, a radiative boundary condition from static model atmospheres, line transfer by scattering, and continuation to supersonic velocities. A Monte Carlo technique determines the theory's eigenvalue J, the mass flux, and the derived J's are in good agreement with the wind models of Pauldrach et al. (2001, A&A, 375, 161). The solutions' sensitivity to the photospheric microturbulent velocity v_t reveals that this parameter has a throttling effect on J: turbulent line-broadening in the quasi-static layers reduces the radiation force available to accelerate matter through the sonic point. If photospheric turbulence approaches sonic velocities, this mechanism reduces mass loss rates by factors $\gtrsim$3, which would partly account for the reduced rates found observationally for clumpy winds.

Key words. stars: early-type – stars: mass-loss – stars: winds, outflows

1. Introduction

The line-driven winds of hot stars are unstable (Lucy & Solomon 1970, [LS70]; Owocki et al. 1988) and the resulting density inhomogeneities strengthen emission lines such as Hα and He II λ4686, thus positively biasing empirical estimates of Φ, the mass-loss rate (Lucy 1975; Abbott et al. 1981). This bias could be corrected if the statistical properties of the inhomogeneities could be predicted, but this is still not feasible. In consequence, clumpiness is now an essential extra parameter in diagnostic analyses of the supersonic outflows from early-type stars (Schmutz 1997; Hillier & Miller 1999). That such investigations confirm clumpiness is no great surprise in view of work in the 1980's concerning X-ray emission, the black troughs of saturated P Cygni lines, and the variability of line profiles. But the magnitude of the concomitant reductions of the inferred Φ's is a major surprise, as is the implication that theory overpredicts Φ's by substantial factors.

The Φ's of Galactic O stars are investigated in the recent papers of Bouret et al. (2005) and Fullerton et al. (2006), both of which also review earlier literature. Bouret et al. analyze the spectra of two O4 stars and derive Φ's that are factors of 3 and 7 below predicted values. On this basis, they conclude that our understanding of mass loss by O stars is in need of fundamental revision.

Fullerton et al. study a much larger sample of 40 stars but, instead of analysing entire spectra, they focus on the P V resonance doublet which, being seldom saturated, more readily yields reliable Φ's than do lines from abundant species. Strong clumping, reducing previous empirical Φ's by factors of 10 or more, is required to match the rates derived from P V. These authors therefore conclude that the "standard model" for hot-star winds needs to be amended.

The theoretical Φ's tested by Bouret et al. (2005) are those derived by Vink et al. (2000) with a refined version of the Monte Carlo (MC) technique of Abbott & Lucy (1985, [AL85]). As such, these Φ's are not eigenvalues of the differential equations governing outflows but are semi-empirical estimates based on an assumed wind structure. Accordingly, if these Φ's are in conflict with observation, the fault may lie in the adopted stratification rather than in the underlying theory.

At present, the closest to a complete theory of radiatively-driven winds is embodied in the code WM-*basic* of Pauldrach et al. (2001). Thus, for a critical test of wind theory, the above reduced empirical Φ's should be compared to the eigenvalues Φ of WM-*basic* models tailored to individual stars. Pending this, some progress is possible with the models in Table 5 of Pauldrach et al. (2001). Interpolation using the Bouret et al. (2005) parameters for HD 190429A gives a WM-*basic* $\Phi \simeq 6.3 \times 10^{-6}\, M_\odot$ yr^{-1}, a factor 3.5 larger than their clumped-wind model. Thus claims that line-driven wind theory is in need of major revision appear to be well founded.

Recent papers on clumpiness confirm what was already evident in the mid 1980's, namely that the "standard model" of line-driven winds must eventually be replaced by 3-D time-dependent gas-dynamical models with simultaneous NLTE radiative transfer. Such models are necessary if we wish to predict from first principles spectral features formed at supersonic velocities. But if clumping is negligible in the neighbourhood of the sonic point, the standard model's predictions of Φ should be fairly accurate since the differential effect of clumpiness at supersonic velocities on the radiation field at the sonic point is surely slight. Thus the evidence that the predicted Φ's are far from accurate perhaps indicates that clumpiness is already significant at the sonic point, a conclusion with some observational support (Bouret et al. 2005).

Notwithstanding this latter possibility, this paper is motivated by the belief that the eigenvalues Φ of stationary-wind solutions should indeed be fairly accurate. Accordingly, the moving reversing layer model of LS70 is revived in order to compute mass fluxes for O star atmospheres and to investigate their sensitivity to assumptions and parameters.

2. An outflowing reversing layer

In this section, the LS70 model of stationary flow accelerating to sonic velocity is updated. The major changes are a vast increase in the line list, a realistic lower boundary condition on

the radiation field, an improved treatment of line formation, and continuation to supersonic velocities. The solution procedure is also changed. Because line formation by pure absorption is replaced by scattering, solution with initial-value integrations is no longer possible. Accordingly, a MC technique akin to that of AL85 is developed.

Despite these improvements, the resulting code falls far short of the physical detail and numerical precision achieved by codes such as WM-*basic*, TLUSTY (Lanz & Hubeny 2003), CMFGEN (Hillier & Miller 1998), and FASTWIND (Puls et al. 2005). But high accuracy is surely not needed in identifying an effect capable of reducing Φ by factors $\gtrsim$3.

2.1. The model

As in LS70, a Schuster-Schwarzschild model is adopted. Thus the lower boundary is a continuum-emitting surface above which is an outflowing plane-parallel isothermal layer where only line- and electron scatterings occur. In addition to chemical composition, the basic parameters are effective temperature $T_{\rm eff}$, surface gravity g, microturbulent velocity $v_{\rm t}$, and mass flux $J = \Phi/4\pi R^2$.

The composition is solar with $N_{\rm He}/N_{\rm H} = 0.1$ (Grevess & Sauval 1998), with the included ions as in Table 1 of Lanz & Hubeny (2003). The temperature of the isothermal flow is set $=0.75T_{\rm eff}$, and H and He are assumed to be fully ionized, so that thermodynamic coefficients are height-independent.

2.2. Gas dynamics

The structure of the reversing layer is determined by the equations governing stationary isothermal flow. With sphericity neglected, the continuity equation has the integral

$$\rho v = J \tag{1}$$

and the equation of motion can then be written as

$$\left(v^2 - a^2\right) \frac{1}{v}\frac{{\rm d}v}{{\rm d}x} = -g_{\rm eff}. \tag{2}$$

Here $a = \sqrt{P/\rho}$ is the isothermal speed of sound and the effective gravity

$$g_{\rm eff} = g - g_{\rm e} - g_\ell \tag{3}$$

where $g_{\rm e}$ and g_ℓ are the radiative accelerations due to electron- and line scatterings, respectively.

From Eq. (2), we see that the sonic point $v = a$ is a critical point at which the velocity gradient is finite only if $g_{\rm eff} = 0$. This condition was used in LS70 to determine the eigenvalue J.

Subsequent to LS70, Castor et al. (1975, [CAK]) pioneered the development of a complete theory of stationary line-driven winds by exploiting the computational economy of the Sobolev approximation. However, the critical point is then no longer at the sonic point but is displaced downstream into the supersonic flow. Here, as in LS70, the Sobolev approximation is not employed. In consequence, g_ℓ is a functional of the solution, and so the critical point remains at the sonic point (Lucy 1975; Poe et al. 1990).

2.3. Stratification

In AL85 and Vink et al. (2000), the MC transfer is performed in an observationally-motivated kinematic model, with Φ determined iteratively by imposing a global dynamical constraint. Here, with the aim of achieving greater local consistency, a family of dynamical models is generated corresponding to an assumed functional form for $g_\ell(v)$. The mass flux J is then determined iteratively by bringing $g_\ell(v)$ and its MC estimator $\tilde{g}_\ell(v)$ into approximate agreement.

The adopted $g_\ell(v)$ is the two-parameter formula

$$g_\ell = g_* \max\left[\delta, \left(\frac{v}{a}\right)^s\right] \quad \text{with} \quad g_* = g - g_{\rm e}. \tag{4}$$

With $0 < \delta < 1$ and $s > 0$, this formula is such that $g_{\rm eff} = 0$ at $v = a$ and is negative at supersonic velocities. The discontinuous derivative of this function at the join of its two segments allows the sharp increase in g_ℓ as the outflow accelerates up to and through the sonic point to be captured.

The solution of Eq. (2) that avoids a singularity at the sonic point has

$$\left(v\frac{{\rm d}v}{{\rm d}x}\right)_a = \frac{1}{2}\left(\frac{{\rm d}\ln g}{{\rm d}\ln v}\right)_a g_* = \frac{1}{2}\, s\, g_*. \tag{5}$$

Accordingly, the velocity law $v(x;\delta,s)$ is derived from Eq. (2) by inward and outward integrations from $v = a$, each with initial derivative given by Eq. (5).

Together with Eq. (1) and the isothermal assumption, $v(x;\delta,s)$ determines the stratification throughout the computational domain (x_0, x_1). The lower boundary x_0 is at electron-scattering optical depth $\tau_{\rm e} = 2/3$ below the sonic point. The upper boundary x_1 is at $v \sim 4a$.

Note that, as in solar-wind theory, the solution has an X-type topology at the critical point. This is assumed without proof because of the difficulty of analysing the solution topology when g_ℓ includes contributions from scattered radiation (Poe et al. 1990).

2.4. Radiation field

The frequency distribution of the continuum intensity I_ν^+ emitted at x_0 is that of the emergent *continuum* flux of the TLUSTY (Lanz & Hubeny 2003) solar-abundance model of the specified $T_{\rm eff}$ and g; the ionization edges due to H and He are therefore accurately represented. The angular distribution is assumed uniform.

At x_1, the integrated flux of the outwardly-directed radiation $I_\nu^+(\mu)$ is constrained to $=\sigma T_{\rm eff}^4$. Correspondingly, $I_\nu^- = 0$ at x_1, so that back-scattering from the highly supersonic flow is neglected. Nevertheless, x_1 is far enough downstream that, for $v \simeq a$, each line's self-interactions with back-scatterings from $v > a$ are treated.

As it propagates through the reversing layer, the continuum is modified by electron scatterings and line transitions. Electron scatterings are assumed to be isotropic but frequency shifts in the co-moving frame (cmf) due to the electrons' thermal motions are taken into account. Following Sect. IIf in AL85, line transitions are treated as resonance scatterings. These are assumed to be isotropic with a re-emitted frequency in the cmf in accordance with complete redistribution. The line profile ϕ_ν comprises a Doppler core due to thermal and microturbulent motions and wings due to radiation damping.

2.5. Ionization and excitation

The treatment of ionization and excitation is designed to give moderately accurate populations for the lower levels of transitions that are major contributors to g_ℓ. Thus the emphasis is on the ground states and low-lying metastable levels of abundant

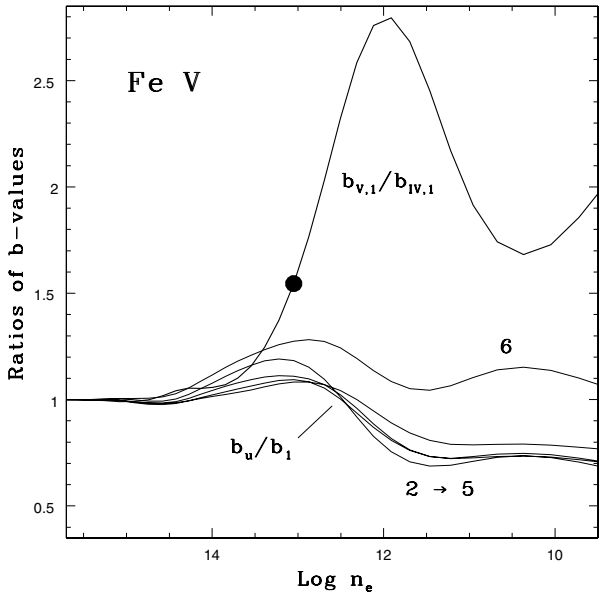

Fig. 1. Ratios of departure coefficients relative to the ground state for selected levels of Fe as functions of n_e for TLUSTY model G50000g400v10.12. Ratios are plotted for superlevels of Fe V with excitation energies <10 eV. Also plotted is the ratio of b-values for the ground states of Fe V and Fe IV. The filled circle is the point where $T_e \simeq 0.75 T_{\rm eff}$.

ions. Conveniently, NLTE departure coefficients for O-star atmospheres can be downloaded from the TLUSTY website, and data from a model with $T_{\rm eff} = 50\,000$ K, log $g = 4$ are plotted in Fig. 1 for the important ion Fe V. This diagram shows the expected convergence to rigorous LTE in deep layers and the growing importance of NLTE in the surface layers. However, because of collisional coupling, the low-lying superlevels of Fe V remain approximately in LTE relative to the ground state. In contrast, for the ionization ratio Fe V/Fe IV, significant departures from LTE occur for $n_e \lesssim 13$ dex. Nevertheless, changes in n_e remain the dominant cause of ionization gradients in the surface layers.

In view of the above, excited levels are assumed to be in LTE with their ground states, whose departure coefficients are fixed at the TLUSTY values in a representative layer. Thus, the ionization equation is

$$\frac{n_{J+1} n_e}{n_J} = \left(\frac{b_{1,J+1}}{b_{1,J}}\right)_\dagger \left(\frac{n_{J+1} n_e}{n_J}\right)^*_\dagger \tag{6}$$

where $*$ denotes LTE and † indicates values for the layer with $T_e \simeq 0.75 T_{\rm eff}$.

2.6. Line list

The basic line data is from Kurucz & Bell (1995). A typical model treats the line formation of $\sim 10^5$ lines in the wavelength interval 228–4000 Å.

3. Monte Carlo code

In this section, a MC code is described for calculating g_ℓ as a function of height in the outflowing reversing layer defined in Sect. 2. The description is brief, focussing on aspects not covered in AL85.

3.1. Discretization

The continuous model derived in Sect. 2 is approximated by ~100 slabs, within each of which ρ and v are constant. The velocity increment between neighbouring slabs is everywhere $\ll v_t$.

3.2. Scattering histories

A total of $\mathcal{N}$ photon packets of energy ϵ_0 are launched into the computational domain at x_0 in time Δt. Their initial rest frame frequencies ν sample the continuum flux distribution of the TLUSTY model and their initial direction cosines are given by $\mu = \sqrt{z}$, where here and below z denotes a random uniform variate obtained with ran2 (Press et al. 1992).

A packet's straight-line trajectory in a slab terminates after travelling distance $s = \min(s_b, s_e, s_\ell)$, where s_b is the distance to the slab's edge, $s_e = -\ln(z)/\sigma_e$, and $s_\ell = -\ln(z)/\ell_{\nu'}$. Here σ_e and $\ell_{\nu'}$ are, respectively, the electron- and line scattering coefficients per unit volume, the latter evaluated at ν', the packet's cmf frequency. Note that these coefficients are constant within each slab.

If the packet undergoes an electron scattering, its new $\mu = 1 - 2z$ and its new ν' is obtained by sampling the angle-averaged redistribution function (Mihalas 1978, p. 432). For a line scattering, the new $\mu = 1 - 2z$ and the new ν' is obtained from the assumption of complete redistribution.

The scattering history of a packet is complete when it exits the computational domain at x_0 or x_1. The number $\mathcal{N}^+$ escaping at x_1 constitute the emergent radiation and so must have an integrated flux corresponding to $T_{\rm eff}$. Thus, at the completion of the MC experiment, the packets' energy ϵ_0 is given by

$$\mathcal{N}^+ \frac{\epsilon_0}{\Delta t} = \sigma T_{\rm eff}^4. \tag{7}$$

3.3. Estimator for g_ℓ

With $\epsilon_0/\Delta t$ from Eq. (7), the MC radiation field, comprising the trajectories of $\mathcal{N}$ packets, can be transformed to physical units and then used to calculate g_ℓ.

If the intensity $I_\nu(x, \mu)$ were known, g_ℓ could be computed from the formula

$$\rho g_\ell = \frac{2\pi}{c} \int_{-1}^{1} \int_0^\infty \ell_{\nu'} I_\nu \mu \, {\rm d}\mu \, {\rm d}\nu \tag{8}$$

valid for $v \ll c$. This can be applied to the energy-packet model using the intensity estimator

$$\tilde{I}_\nu \, {\rm d}\nu \, {\rm d}\omega = \frac{\epsilon_0}{\Delta t} \frac{1}{V} \sum_{{\rm d}\nu {\rm d}\omega} \frac{\epsilon_\nu}{\epsilon_0} \, s \tag{9}$$

where the summation is over all pathlength segments s in the reference volume V of packets in $(\nu, \nu + {\rm d}\nu)$ propagating in solid angle element ${\rm d}\omega$. This formula is derived in Lucy (2005) and repeated in order to correct a typographical error. Equation (9) relates the energy-packet and the specific-intensity representations of radiation.

In the present application, $v \ll c$ and so setting $\epsilon_\nu = \epsilon_0$ is an excellent approximation. Also the geometry is plane-parallel, so V is a column of unit cross-section and length Δx, the slab's width. Substitution into Eq. (8) then gives the estimator

$$\rho \tilde{g}_\ell = \frac{1}{c} \frac{\epsilon_0}{\Delta t} \frac{1}{\Delta x} \sum \ell_{\nu'} \, \mu \, s \tag{10}$$

where the summation is over all trajectories in the slab.

This optimum estimator for g_ℓ exploits all the information in the packets' trajectories. This would not be the case if g_ℓ were derived from the momentum transfers occurring when packets undergo line scatterings. Even if no line scatterings occur in a slab, Eq. (10) returns a non-zero $\tilde{g}_\ell$, provided only that at least one packet propagates with a ν' at which $\ell_{\nu'} \neq 0$.

Because this calculation of g_ℓ does not rely on the Sobolev approximation, the effects of scattered radiation discussed by Owocki & Puls (1999) are included. Moreover, line-profile overlapping and multiline transfer are accurately treated. These effects are excluded when Sobolev theory is used in the narrow-line limit with the assumption that each line interacts with unattenuated continuum.

3.4. Computational economy

With the procedure as described, a prohibitive amount of computer time would be required for an accurate $\tilde{g}_\ell$. Accordingly, two simplifications are introduced.

A MC treatment of re-emission with complete redistribution should first randomly select which of the overlapping lines contributing to $\ell_{\nu'}$ is the actual absorber and then sample its profile $\phi_{\nu'}$ to select the ν' of the emitted packet. This has been simplified by always taking the absorber to be the largest contributor to $\ell_{\nu'}$, which is identified when $\ell_{\nu'}$ is tabulated prior to the MC calculation. Little loss of accuracy is expected since absorption usually occurs in a line's Doppler core and this typically strongly dominates the damping wings of neighbouring transitions.

The second simplification avoids trapping in the Doppler cores of strong lines. A photon undergoing numerous scatterings in a Doppler core is described by Rybicki & Hummer (1969) as being imprisoned at a point and from which it escapes only when the low probability event of emission in the damping wings occurs. When a MC packet is similarly imprisoned, its escape via the damping wings is expedited. The actual procedure is as follows: with standard notation, the Voigt profile is approximated (Mihalas 1978, p. 281) by the Gaussian core when $|v| < v^*$ and by the damping wings when $|v| > v^*$, where v^* is such that the two terms are equal. If a slab is optically thick in a Doppler core, the next re-emission is forced to occur in the wings. Since $\phi_\nu \propto 1/v^2$ in the wings, a random $v = \pm v^*/z$.

4. Examples

In this section, moving reversing layers are derived for the three TLUSTY atmospheres with parameters matching those of models in Table 5 of Pauldrach et al. (2001). Mass fluxes can then be compared without interpolation, thereby testing the approximations used to construct the simple code described in Sects. 2 and 3.

4.1. Parameter fitting

With $T_{\rm eff}, g$ and composition fixed, the remaining parameters are J, δ, s and $v_{\rm t}$. In the WM-*basic* models, $v_{\rm t}$ increases from 10 km s^{-1} at the photosphere to $0.1 v_\infty$ in the terminal flow. Here, we ignore this gradient and set $v_{\rm t} = 10$ km s^{-1}.

With a trial parameter vector (J, δ, s), a MC calculation is carried out as described in Sect. 3. Equation (10) then gives $\tilde{g}_\ell$ throughout the reversing layer and thus allows us to see how closely the assumed $g_\ell(v)$ given by Eq. (4) is recovered. The goodness-of-fit is quantified by calculating

$$\eta = \frac{1}{I} \sum \left| \frac{\tilde{g}_\ell - g_\ell}{g_\ell} \right| \tag{11}$$

where the summation is over the I slabs with $0.25 < v/a < 1.75$. Velocities outside this interval are excluded to avoid the edge effects due to imperfect boundary conditions.

With many repetitions of this procedure, the vector (J, δ, s) minimizing η can be found. In the initial search, models are calculated with $\mathcal{N} = 10^7$, but this is increased to 4×10^7 in the close neighbourhood of the minimum and then further increased to $\mathcal{N} \gtrsim 10^8$ for the illustrations herein.

Since the interval $(0.25, 1.75)$ includes the sonic point, the regularity condition at $v = a$ is satisfied exactly if $\eta = 0$. But because of MC sampling errors and the limited flexibility of the formula for g_ℓ, this is not achievable. Accordingly, minimizing η replaces the condition $g_{\rm eff} = 0$ at $v = a$ as the criterion determining the eigenvalue J.

4.2. Model D-50

Model D-50 of Pauldrach et al. (2001) has $T_{\rm eff} = 50\,000$ K, $\log g = 4$, $R/R_\odot = 12$, and $\Phi = 5.6 \times 10^{-6}\ M_\odot$/yr, corresponding to a photospheric mass flux $J(\mathrm{gm\ s^{-1}}) = -4.40$ dex . The matching TLUSTY model is G50000g400v10.12, details of which were used for Fig. 1. From the emergent spectrum of this model, continuum fluxes were estimated at intervals of 0.1 in $\log \nu$ and at both sides of ionization edges. Linear logarithmic interpolation then defines the ν-distribution of I_ν^+ at x_0.

The best-fit moving reversing layer has parameter vector $(\log J, \delta, s) = (-4.41, 0.61, 2.03)$ which gives $\eta = 0.048$, and this fit worsens with displacement vectors $(\pm 0.05, \pm 0.03, \pm 0.05)$. Thus the mass flux of this model agrees with the WM-*basic* model to within 0.05 dex.

The success in reproducing the assumed g_ℓ is shown in Fig. 2. The agreement is seen to be excellent from $v \simeq 10$ to $\simeq$70 km s^{-1}, an interval containing the sonic point at 22.6 km s^{-1}. In particular, the discontinuity in the derivative of $g_\ell(v)$ at $v = 17.5$ km s^{-1} closely matches a sharp change in the slope of $\tilde{g}_\ell(v)$. On the other hand, the fit is less successful for $v \lesssim 10$ km s^{-1}, where Eq. (4) reduces to $g_\ell = g_* \delta$.

4.3. Model D-40

Model D-40 of Pauldrach et al. has $T_{\rm eff} = 40\,000$ K, $\log g = 3.75$, $R/R_\odot = 10$, and $\Phi = 0.24 \times 10^{-6}\ M_\odot$/yr, corresponding to $J(\mathrm{gm\ s^{-1}}) = -5.60$ dex . In this case, the source of b-values at the representative point and of the continuum-flux distribution is the TLUSTY model G40000g375v10.12.

The best-fit moving reversing layer for $v_{\rm t} = 10$ km s^{-1} has $(\log J, \delta, s) = (-5.65, 0.58, 2.55)$, with $\eta = 0.048$. Thus the mass flux is lower than that of the WM-*basic* model by a barely significant 0.05 dex.

4.4. Model S-30

Model S-30 has $T_{\rm eff} = 30\,000$ K, $\log g = 3.00$, $R/R_\odot = 27$, and $\Phi = 5.0 \times 10^{-6}\ M_\odot$/yr, corresponding to $J(\mathrm{gm\ s^{-1}}) = -5.15$ dex. The matching TLUSTY model is G30000g300v10.12.

The best-fit moving reversing layer for $v_{\rm t} = 10$ km s^{-1} has $(\log J, \delta, s) = (-5.45, 0.79, 1.75)$, with $\eta = 0.072$. Thus the mass flux is lower than that of the WM-*basic* model by an apparently

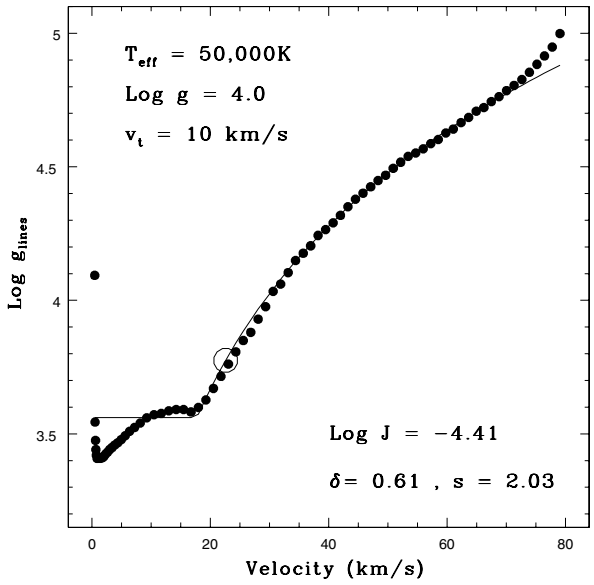

Fig. 2. Comparison of radiative accelerations due to lines. The filled circles are values given by the MC estimator $\tilde{g}_\ell$, and the solid line is the function $g_\ell(v)$ assumed in deriving the reversing layer's stratification. The open circle indicates the sonic point.

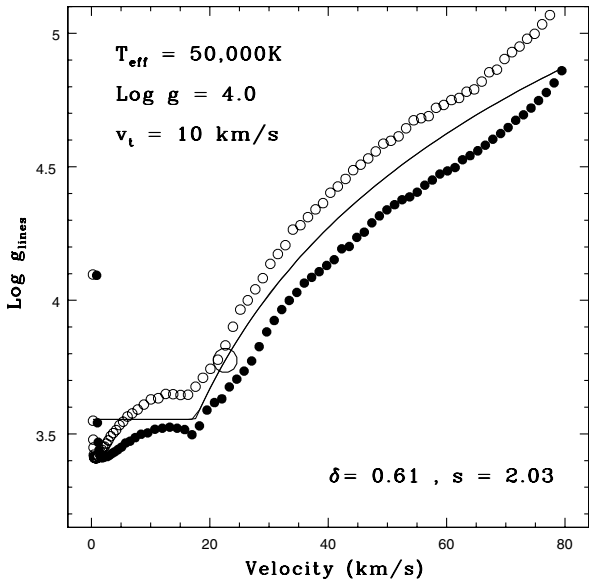

Fig. 3. Effect of varying mass flux J, with other parameters as in Fig. 2. The filled and open circles are values of $\tilde{g}_\ell$ when $J(\mathrm{gm\,s^{-1}}) = -4.11$ and -4.71 dex, respectively The solid line is the function $g_\ell(v)$ assumed in deriving the reversing layer's stratification, and the large open circle indicates the sonic point.

significant 0.3 dex. However, the reliability of this model has been questioned (Puls et al. 2005, p. 686).

4.5. Consistency checks

The good agreement of the J's with those of the reliable WM-*basic* models provides strong support for the simplifying assumptions introduced in Sects. 2 and 3. A further consistency check is obtained from the lines contributing to $\tilde{g}_\ell$. The treatment of ionization and excitation in Sect. 2.5 focuses on low-lying energy levels in the expectation that the bulk of the radiative driving derives from scattering by such levels. This is tested for the layer with $v \simeq a$ in model D-50. For this layer, $\tilde{g}_\ell \simeq g_*$, with the fractions 0.70 and 0.88 arising from levels with excitation energies <5 and <10 eV, respectively.

5. Variation of parameters

In this section, insight is sought into the behaviour of moving reversing layers by varying parameters.

5.1. Mass flux

The excellent fit of $\tilde{g}_\ell$ to g_ℓ in Fig. 2 is lost if parameters change. In Fig. 3, the effects of the displacements $\Delta J = \pm 0.3$ dex are shown. The changes in $\tilde{g}_\ell$ are in the expected sense. Thus an increase in J results in a $\tilde{g}_\ell$ that falls below the assumed $g_\ell(v)$ and is therefore incapable of accelerating the outflow.

Figure 3 supports the assumption of an X-type topology since there is no hint of the solution indeterminacy characteristic of a nodal-type topology (Poe et al. 1990). The sensitivity to mass flux is consistent with there being a unique eigenvalue J for which there is a stationary outflow accelerating from sub- to supersonic velocities.

5.2. Microturbulence

In a second sensitivity experiment, the effect of varying v_t is investigated. Figure 4 plots $\tilde{g}_\ell(v)$ for $v_\mathrm{t} = 6.7$ and 15 $\mathrm{km\,s^{-1}}$. In this case, the results are less readily anticipated.

For $v \lesssim 15\ \mathrm{km\,s^{-1}}$, $\tilde{g}_\ell$ increases with v_t. This is a consequence of the broadened lines in the quasi-static layers intercepting an increased fraction of the continuum. A simple analysis of this effect is given in Sect. IIb of LS70. With a slowly-varying logarithmic factor neglected, this analysis shows that, in a static atmosphere with a fixed column density of absorbing ions, a strong resonance line has $g_\ell \propto \Delta\nu_D$, which is $\propto v_\mathrm{t}$ when microturbulence dominates the ions' thermal motions.

Following a crossover at $v \simeq 20\ \mathrm{km\,s^{-1}}$, this dependency is reversed and $\tilde{g}_\ell$ becomes an decreasing function of v_t. This is again a consequence of the broadening of lines formed in the quasi-static layers. Continuum radiation that would have been available to accelerate matter moving with $v \sim 30$–$40\ \mathrm{km\,s^{-1}}$ has already been partly absorbed in the turbulent flow at subsonic bulk velocities.

The final feature to be explained is the convergence of the $\tilde{g}_\ell$ plots for $v \gtrsim 60\ \mathrm{km\,s^{-1}}$. This is the Sobolev regime. Matter has been accelerated from out of the shadow of lines formed in the quasi-static flow and the narrow-line limit is approached in which g_ℓ becomes independent of ϕ_ν and therefore of v_t.

With Fig. 4 understood, the next point of interest is the change in (J, δ, s) required to recover a good fit between $\tilde{g}_\ell$ and g_ℓ. The above discussion indicates that as v_t increases so will δ, as lines then provide more support for the quasi-static layers, but J will decrease to compensate for the reduced flux available to accelerate matter through the sonic point.

For each of the three WM-*basic* models considered in Sect. 4, a sequence of best-fit models with varying v_t is given in Table 1. Each sequence has the continuum flux distribution and the b-values of the TLUSTY model identified in Sects. 4.2–4.4. In consequence, there is an inconsistency since the TLUSTY models assume $v_\mathrm{t} = 10\ \mathrm{km\,s^{-1}}$. But the dominant effects of v_t on the parameter vector are surely those just discussed. Note

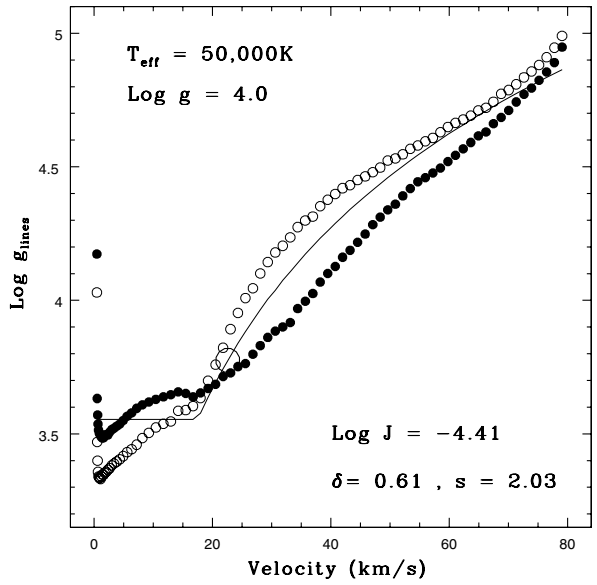

Fig. 4. Effect of varying microturbulent velocity v_t, with other parameters as in Fig. 2. The filled and open circles are values of $\tilde{g}_\ell$ when $v_t = 15$ and 6.7 km s^{-1}, respectively The solid line is the function $g_\ell(v)$ assumed in deriving the reversing layer's stratification, and the large open circle indicates the sonic point.

Table 1. Models with varying microturbulence.

Model	v_t	δ	s	$\log J$	$\eta \times 100$
D-50	6.7	0.48	1.96	–4.09	2.6
	10.0	0.61	2.03	–4.41	4.8
	15.0	0.69	1.59	–4.71	10.3
	22.5	0.80	1.15	–5.00	10.4
D-40	6.7	0.52	2.30	–5.34	8.5
	10.0	0.58	2.55	–5.65	4.8
S-30	6.7	0.74	2.20	–5.15	6.1
	10.0	0.79	1.75	–5.45	7.2

that the effect of v_t on line-blocking and hence backwarming is approximately accounted for by Eq. (7). Thus, because packets that re-enter the photosphere are implicitly thermalized and re-radiated, the continuum flux at x_0 exceeds $\sigma T_{\rm eff}^4$ by an amount that depends on v_t.

From Table 1, we see that δ and J vary in the sense expected. In particular, J decreases by $\simeq$0.3 dex as v_t increases by 0.18 dex, corresponding to a power-law exponent of -1.7. However, although this effect is readily understood and undoubtedly real, the quality of the fits is markedly poorer for the D-50 models with $v_t = 15$ and 22.5 km s^{-1}. This indicates the need for a more complicated fitting function $g_\ell(v)$ to replace Eq. (4).

Turbulent broadening is treated here in the microturbulent limit in which the length scale of random velocity fluctuations is $\ll$ the mean free paths of line photons. But the mechanism does not require this assumption: any photospheric line-broadening that reduces ρg_ℓ at $v \simeq a$ will contribute to this throttling effect. In particular, therefore, turbulence with length scales up to $\sim$ the photospheric scale height might well be important, and there is strong observational evidence (Conti & Ebbets 1977; Howarth et al. 1997) for turbulent velocities well in excess of the standard $v_t \simeq 10$ km s^{-1} required by line strengths.

6. Discussion

The above calculations reveal a fundamental coupling between line formation in the quasi-static photospheric layers and the mass flux J that can be accelerated to supersonic velocities. This low-velocity, non-Sobolev effect must be accurately treated when J or Φ are computed as eigenvalues of the equations of stationary line-driven winds.

6.1. Previous work

This coupling was already recognized in LS70. In Fig. 2 of that paper, the precipitous drop of J at $\log T_{\rm eff} \simeq 4.5$ was attributed to the absorption of radiation at $\nu_i(1 + a/c)$ by the damping wings of the C IV doublet. Here, with the inclusion of numerous weak lines, J falls less precipitously when photospheric line broadening reduces the contributions of strong lines to ρg_ℓ at $v \simeq a$. Moreover, rather than damping wings, turbulent broadening of Doppler cores is a more plausible cause of a reduced radiation force in the transonic flow.

Because the throttling effect of turbulent broadening requires non-Sobolev line transfer, it is absent from CAK theory. The ion thermal speed $v_{\rm th}$ that appears in CAK formulae is for dimensional reasons and scales out when derived properties are expressed in physical units (Abbott 1982; Poe et al. 1990).

The hydrodynamic structure of WM-*basic* models are obtained with CAK theory and thus a dependence of the eigenvalue Φ on photospheric turbulence would seem to be excluded. However, the CAK force multiplier parameters are iteratively adjusted to fit g_ℓ given by a detailed NLTE transfer code that assumes a velocity-dependent microturbulence with $v_t = 10$ km s^{-1} at the photosphere. Although this introduces a dependence of Φ on v_t, the displacement of the CAK critical point into the supersonic flow suggests that the throttling effect will be less powerful than found here. But if the CAK formalism were eliminated and the stratification derived directly from the gas dynamic equations with critical point at the sonic point, an accurate treatment of the dependence of Φ on v_t would be possible with this code.

Although not identified with turbulence, the throttling effect of an enhanced $v_{\rm th}/a$ is evident in the pure absorption calculations reported by Poe et al. (1990). Moreover, they summarize the implications of this parameter for time-dependent simulations and the uniqueness of stationary solutions.

Hillier et al. (2003) identify the treatment of microturbulence in calculating ρg_ℓ near the sonic point as a major unsolved issue and recognize that the Poe et al. work can be re-interpreted to anticipate the effects of microturbulence.

6.2. Calculating Φ

Two theoretical techniques for computing Φ have emerged, one fundamental, the other semi-empirical. The fundamental approach determines Φ or J as an eigenvalue of the governing differential equations by demanding regularity at the critical point. The semi-empirical approach, on the other hand, determines Φ algebraically by demanding that the flux of mechanical energy in the terminal flow should be accounted for by the loss of radiative luminosity due to line- and electron scatterings in the outflowing matter.

A consequence of this investigation is that the fundamental approach is harder than hitherto realized. An essential phenomenon, photospheric turbulence, is not predictable as yet from first principles and only measurable with moderate accuracy, even in the favourable but unlikely circumstances that such

motions are restricted to the microturbulent limit and do not vary with height. Accordingly, by default, the semi-empirical technique is currently preferable as a source of Φ's for input into other astrophysical investigations. The details of transonic flow are then inconsequential because the kinetic energy per gm at the sonic point is negligible compared to that of the terminal flow ($v_\infty^2/2$) which, moreover, is an observable.

As discussed in Sect. 1, the semi-empirical Φ's obtained by Vink et al. (2000) are too high according to Bouret et al. (2005). This may well be because the AL85 assumptions of laminar flow with a monotonic velocity law are retained. But these assumptions are not fundamental to the MC technique. The Vink et al. (2000) investigation could usefully be repeated with the stratification updated in accordance with the already cited papers on clumpiness as well as the recent papers of Puls et al. (2006) and Oskinova et al. (2006). Moreover, the treatment of line formation could be improved to treat branching (Sim 2004).

A survey of Φ's for hot stars could also be carried out with the diagnostic code CMFGEN, which already incorporates clumpiness and random non-monoticity. For radii where the bulk velocity $v(r)$ is highly supersonic, we have to a good approximation

$$\frac{1}{2}v^2 = \int_R^r (g_\ell - g_*)\mathrm{d}r. \tag{12}$$

By demanding that this equation is satisfied at $r = \infty$, Φ could be determined algebraically in a manner analogous to AL85 and Vink et al. (2000). Further wind parameters, such as β in the velocity law, could be determined by minimizing violations of this equation over its range of validity.

7. Conclusion

The aim of this paper has been to examine claims that the theory of line-driven winds overpredicts mass loss rates. To this end, the theory of moving reversing layers has been updated and used to investigate the sensitivity of transonic flow to input parameters. The reported calculations reveal that photospheric turbulence, by reducing the driving force at the sonic point, plays a decisive role in regulating the mass flux of stationary flow. Codes that compute Φ as an eigenvalue will therefore overpredict if turbulent line-broadening is underestimated. This may occur as a result of observational underestimates of v_t or because the microturbulent limit is violated. A further possible cause of overprediction is reliance on the CAK critical point in determining the eigenvalue. Because this point is at supersonic velocity, the throttling effect of photospheric turbulence is likely to be reduced, a topic meriting further research.

The calculations presented in Table 1 suggest the conjecture that the mass loss rates of hot stars are less than predicted because of the throttling effect of photospheric turbulence. With the critical point at the sonic point as required by non-Sobolev line transfer, this effect reduces J for stationary flow by a factor $\gtrsim$3 for near sonic turbulence.

However, additional work is required to establish this conjecture. The MC technique presented herein is barely adequate for computing J's when $v_\mathrm{t} \gtrsim 15\ \mathrm{km\,s^{-1}}$. Repetition with an improved parameterization of g_ℓ or solution with an alternative procedure is therefore desirable. But, more fundamentally, the conjecture is motivated by the behaviour of stationary solutions, and these are unstable (Sect. 1). Ultimately, therefore, as the referee remarks, time-dependent calculations are needed to see if the time-averaged J is similarly constrained by photosperic turbulence.

With regard to analyses of individual stars, the eigenvalue $\Phi = 4\pi R^2 J$ obtained from a moving reversing layer computed with the spectroscopic v_t should be compared with the empirical Φ obtained from the supersonic wind with clumpiness and non-monoticity included. Such analyses could usefully exploit the wide range of v_t's reported for O stars (Bouret et al. 2003; Heap et al. 2006).

Acknowledgements. I am grateful to the referee, J. Puls, for detailed comments on the original version.

References

Abbott, D. C., Bieging, J. H., & Churchwell, E. 1981, ApJ, 250, 645
Abbott, D. C. 1982, ApJ, 259, 282
Abbott, D. C., & Lucy, L. B. 1985, ApJ, 288, 679 (AL85)
Bouret, J.-C., Lanz, T., Hillier, D. J., et al. 2003, ApJ, 595, 1182
Bouret, J.-C., Lanz, T., & Hillier, D. J. 2005, A&A, 438, 301
Castor, J. I., Abbott, D. C., & Klein, R. I. 1975, ApJ, 195, 157 (CAK)
Conti, P. S., & Ebbets, D. 1977, ApJ, 213, 438
Fullerton, A. W., Massa, D. L., & Prinja, R. K. 2006, ApJ, 637, 1025
Grevess, N., & Sauval, A. J. 1998, Sp. Sci. Rev., 85, 161
Heap, S. R., Lanz, T., & Hubeny, I. 2006, ApJ, 638, 409
Hillier, D. J., & Miller, D. L. 1998, ApJ, 496, 407
Hillier, D. J., & Miller, D. L. 1999, ApJ, 519, 345
Hillier, D. J., Lanz, T., Heap, S. R., et al. 2003, ApJ, 588, 1039
Howarth, I. D., Siebert, K. W., Hussain, G. A. J., & Prinja, R. K. 1997, MNRAS, 284, 265
Rybicki, G. B., & Hummer, D. G. 1969, MNRAS, 144, 313
Kurucz, R. L., & Bell, B. 1995, Kurucz CD-ROM No. 23
Lanz, T., & Hubeny, I. 2003, ApJS, 146, 417
Lucy, L. B., & Solomon, P. M. 1970, ApJ, 159, 879 (LS70)
Lucy, L. B. 1975, Mem. Soc. R. Sci. Liège, 8, 359
Lucy, L. B. 2005, A&A, 429, 19
Oskinova, L. M., Feldmeier, A., & Hamann, W.-R. 2006, MNRAS, 372, 313
Owocki, S. P., Castor, J. I., & Rybicki, G. B. 1988, ApJ, 335, 914
Owocki, S. P., & Puls, J. 1999, ApJ, 510, 355
Pauldrach, A. W. A., Hoffmann, T. L., & Lennon, M. 2001, A&A, 375, 161
Poe, C. H., Owocki, S. P., & Castor, J. I. 1990, ApJ, 358, 199
Press, W. H., Teukolsky, S. A., Vetterling, W. T., & Flannery, B. P. 1992, Numerical Recipes (Cambridge: Cambridge Univ. Press)
Puls, J., Urbaneja, M. A., Venero, R., et al. 2005, A&A, 435, 669
Puls, J., Markova, N., Scuderi, S., et al. 2006, A&A, 454, 625
Schmutz, W. 1997, A&A, 321, 268
Sim, S. 2004, MNRAS, 349, 899
Vink, J. S., de Koter, A., & Lamers, H. J. G. L. M. 2000, A&A, 362, 295